cmgh
CELLULAR AND MOLECULAR GASTROENTEROLOGY AND HEPATOLOGY

ORIGINAL RESEARCH

ZnT2-Mediated Zinc Import Into Paneth Cell Granules Is Necessary for Coordinated Secretion and Paneth Cell Function in Mice

Abigail B. Podany,[1,2] Justin Wright,[3] Regina Lamendella,[3] David I. Soybel,[1,2] and Shannon L. Kelleher[1,2,4]

[1]Department of Surgery, [2]Department of Cellular and Molecular Physiology, and [4]Department of Pharmacology, Penn State Hershey College of Medicine, Hershey, Pennsylvania; [3]Department of Biology, Juniata College, Huntingdon, Pennsylvania

SUMMARY

The current study determined that zinc transporter (ZnT)2 was responsible for Zn uptake into Paneth cell granules. Moreover, loss of ZnT2 function in ZnT2-null mice impaired Paneth cell function and granule structure, secretion, and antimicrobial activity, which led to gastrointestinal dysbiosis.

BACKGROUND & AIMS: Defects in Paneth cell (PC) function are associated with microbial dysbiosis and intestinal inflammation. PC granules contain antimicrobial peptides, cytokines, and substantial stores of zinc (Zn). We hypothesized that Zn, transported into the granule through the Zn transporter (ZnT)2, is critical for signature PC functions.

METHODS: ZnT2 was localized to PC granules using immunofluorescence and sucrose gradient fractionation in wild-type (*wt*) mice, and consequences of ZnT2 loss were characterized in ZnT2 knockout (*ZnT2ko*) mice. Terminal ilea were harvested for immunofluorescence, electron microscopy, and fluorescent imaging with the Zn reporter Zinpyr-1. Alterations in fecal microbiota were characterized using 16s ribosomal RNA sequencing. PC degranulation, bacterial translocation, cytokine response to *Escherichia coli* endotoxin lipopolysaccharide, crypt viability after exposure to the oxidant monochloramine (NH_2Cl), and bactericidal activity of luminal contents of terminal ilea against enteropathogenic *E coli* were assessed.

RESULTS: ZnT2 was localized to the membrane of PC granules. In *ZnT2ko* mice, spontaneous degranulation was observed more frequently than among *wt* mice. Secretory granules were hypodense with less active lysozyme, and there was evidence of autophagosome accumulation and granule degradation in PCs from *ZnT2ko* mice. Gut microbiota of *ZnT2ko* mice were enriched in *Bacteroidales* S24-7 and relatively depleted of species commonly found in *wt* mice. Evidence of PC dysfunction in *ZnT2ko* mice included impaired granule secretion and increased inflammatory response to lipopolysaccharide, less bactericidal activity, and greater susceptibility to cell death from NH_2Cl.

CONCLUSIONS: ZnT2 is critical for Zn import into PC granules, and the inability to import Zn leads to profound defects in PC function and uncoordinated granule secretion. *(Cell Mol Gastroenterol Hepatol 2016;2:369–383; http://dx.doi.org/10.1016/j.jcmgh.2015.12.006)*

Keywords: Small Intestine; Zinc Transporter; Microbiota.

Paneth cells (PCs) are highly specialized secretory epithelial cells that reside in the crypts of Lieberkühn of the small intestine.[1,2] Implicated in the development of the intestine and conservation of the mucosal barrier, PCs also play a critical role in regulating the ecology of the intestinal lumen through release of large secretory granules that contain antimicrobial proteins (eg, α-defensin, lysozyme, and Reg-IIIγ), cytokines (eg, interleukin [IL]17 and tumor necrosis factor [TNF]), and growth factors (eg, epidermal growth factor).[1,3–5] Defects in PC function result in impairments in defensin formation, defects in secretory or autophagic pathways,[2] and are associated with microbial dysbiosis and inflammatory bowel conditions such as necrotizing enterocolitis (NEC) and Crohn's disease.[1,6]

It has long been recognized that PC granules contain remarkably high levels of zinc (Zn).[7,8] Zn is a cofactor for granule enzymes such as matrix metalloproteinase-7 and provides stability for α-defensin 5[9] and lysozyme.[10,11] Recent studies in rodents have indicated that depletion of Zn in the small intestine renders PCs susceptible to cell death,[12,13] and can lead to downstream disruption of the intestinal stem cell niche.[13] In mice, depletion of Zn in the PC, combined with exposure to intestinal pathogens such as *Klebsiella pneumoniae*, results in an illness similar to the NEC that is observed in preterm newborns.[14] These observations suggest that Zn is

Abbreviations used in this paper: **CFU, colony forming unit; EPEC, enteropathogenic *Escherichia coli*; ER, endoplasmic reticulum; IF, immunofluorescent; IL, interleukin; IP, intraperitoneal; ko, knockout; LPS, lipopolysaccharide; NEC, necrotizing enterocolitis; OTU, organizational taxonomic unit; PBS, phosphate-buffered saline; PC, Paneth cell; PCR, polymerase chain reaction; TNF, tumor necrosis factor; wt, wild-type; ZIP, ZRT, IRT-like protein; Zn, zinc; ZnT, zinc transporter.**

Most current article

2352-345X
http://dx.doi.org/10.1016/j.jcmgh.2015.12.006

critical for PC viability and functionality of its granules. How Zn is incorporated into PC granules and why defects in granule Zn accumulation impair PC function are not understood.

Movement of Zn into and through secretory cells is dominated by 2 families of Zn transporters.[15,16] Members of the *SLC30A* family of Zn transporters (ZnT1–10) function as homodimers and heterodimers[17] to move Zn out of the cytoplasm into organelles or across the cell membrane to extracellular compartments. Four members the ZnT family (ZnT2, ZnT3, ZnT4, and ZnT8) have been described in the secretory compartments of specialized secretory tissues including mammary gland, prostate, exocrine pancreas, endocrine pancreas, and neurons.[18–22] Of these, ZnT3 and ZnT8 are distinguished by almost exclusive expression in neural cells and pancreatic islets, respectively.[16,18,20,22] Although ZnT4 is expressed in the gastrointestinal system, predominant expression occurs in the large intestine and in nonapical endosomal compartments of the enterocyte.[23,24] In contrast, expression of ZnT2 in secretory epithelial tissues (eg, mammary gland, prostate, the exocrine acinar cells of the pancreas[19,25–28]) and in the crypts of Lieberkühn[29] suggests that ZnT2 may play a role in Zn accumulation in PC granules.

Recent reports have suggested that functionally significant mutations[30,31] and nonsynonymous genetic variants[32] in ZnT2 are common, offering the possibility that variation in ZnT2 might be important in regulating responsiveness in secretory cells and tissues. These considerations led us to test the hypothesis that ZnT2 is responsible for Zn import into PC granules and that silencing ZnT2 would impair PC function, resulting in dysbiosis within the lumen of the small intestine. Here, we used a ZnT2-null mouse model to evaluate the role of this Zn transporter in PC function, and the consequences of loss of ZnT2 function on luminal dysbiosis and response to infectious stimuli.

Materials and Methods

Animals

All animal protocols were approved by the Institutional Animal Care and Use Committee at the Pennsylvania State University. Male ZnT2-null (*ZnT2 knockout* [*ko*]) mice and their wild-type (*wt*) littermates (10–12 wk) were obtained through heterozygote breeding, maintained on a 12-hour light/dark cycle under controlled temperature and humidity, and given access to commercial rodent chow and water ad libitum. DNA was extracted from ear snips following the manufacturer's instructions using the Extract-N-Amp Tissue polymerase chain reaction (PCR) kit (Sigma-Aldrich, St. Louis, MO) and lack of ZnT2 was confirmed by PCR genotyping as previously described.[26] Lack of ZnT2 protein in the crypts was confirmed by immunoblotting as described later.

General Characterization

Mice (n = 8/genotype) were fasted for 2 hours and euthanized by CO_2 asphyxiation and the terminal third of their small intestines (ileum) was removed and processed for crypt isolation, histology, Zn analysis, and immunoblotting as described later. Blood was removed by cardiac puncture into heparinized tubes and plasma was separated by centrifugation in a Marathon Micro H centrifuge (Fisher Scientific, Waltham, MA) at 2000 × g for 5 minutes. Plasma was stored at -20°C until analysis for Zn concentration as described later.

Lipopolysaccharide Injection

Mice (n = 5/genotype) were fasted for 2 hours before intraperitoneal (IP) injection of lipopolysaccharide (LPS) (1 mg/kg) or saline (control). After 3 hours, mice (LPS, n = 3; saline, n = 2) were euthanized by CO_2 asphyxiation and terminal ilea were harvested and processed for H&E staining, transmission electron microscopy, and immunoblotting as described later. A second cohort of mice (LPS, n = 3; saline, n = 3) treated as described earlier were euthanized by CO_2 asphyxiation after 24 hours to obtain mesenteric lymph nodes, which were isolated for bacteriologic culture. From these animals, spleens were harvested for quantification of splenic cytokines as described later.

Light Microscopy

Ileum (n = 8 mice/genotype) was dissected and perfused with 2 mL sterile phosphate-buffered saline (PBS), followed by 4% phosphate-buffered paraformaldehyde, pH 7.4. Tissues were embedded in paraffin, sections (5 μm) were adhered to positively charged glass slides, deparaffinized, and used for H&E, alcian blue, and immunofluorescent (IF) staining.

H&E and alcian blue staining. Sections from *wt* and *ZnT2ko* mice (n = 8 mice/genotype) were stained with H&E and alcian blue as described.[33,34] Morphology and morphometrics were assessed in high-quality sections containing full villi. At least 20 crypts and villi were assessed per mouse by a single blinded observer. Villus height, crypt depth, nuclei per villus, and the number of goblet cells per villus were measured or counted at 10× magnification as described.[34,35] Villus height was measured by drawing a bisecting line through the center of the villi, and crypt depth was measured by drawing a bisecting line through the crypt lumen using Adobe Photoshop CS3 version 10.0 (Adobe Systems Incorporated, San Jose, CA). PC organization was examined at a magnification of 63× under oil. At least 100 PCs per mouse (n = 6/genotype) were quantified for degree of degranulation as previously described.[2] Briefly, PCs were rated according to their appearance based on the schematic representation of degranulation (grades D0–D3), as adapted from Adolph et al[2] by 2 independent, blinded observers.

Immunofluorescent (IF) staining. Sections from *wt* and *ZnT2ko* mice (n = 4–6 mice/genotype) were used for IF staining. Antibodies used were as follows: anti–8-hydroxydeoxyguanosine (20 μg/mL, ab62623; Abcam, Cambridge, MA), ZnT2 (4 μg/mL, sc-27507; Santa Cruz Antibody, Santa Cruz, CA), Reg-IIIγ (1:100; a gift from Dr Matam Vijay-Kumar), Bmi-1 (12 μg/mL, ab38295; Abcam), and Lgr-5 (1:25, ab75732; Abcam). Primary antibodies were visualized with donkey anti-goat IgG Alexa Fluor 488 (4 μg/mL, A11055; Life Technologies, Frederick, MD), donkey anti-rabbit IgG Alexa Fluor 594 (4 μg/mL, A21207; Life

Technologies), or anti-mouse IgG Alexa Fluor 488 (4 μg/mL, A21202; Life Technologies), and counterstained with 4',6-diamidino-2-phenylindole (175 μg/mL; Life Technologies). Images were collected at 20×, 40×, or under oil at 63× magnification using a Leica DM IL LED microscope with a Leica DFC425 digital camera (Leica Microsystems, Buffalo Grove, IL) or using a Leica Inverted Confocal Microscope SP8 (Leica Microsystems). Images were collected using Leica Application Suite (V3.6) and saved as .tiff files. Brightness was adjusted uniformly across all images using Adobe Photoshop CS3 version 10.0.

Transmission Electron Microscopy

The terminal ileum (n = 9 mice/genotype; 4/genotype with no treatment; 2/genotype with IP injection of saline; and 3/genotype with IP injection of LPS) was dissected, perfused, and fixed with half-strength Karnovsky's fixative (2% paraformaldehyde, 2.5% glutaraldehyde in 0.2 mol/L sodium cacodylate buffer at pH 7.4 at 4°C) for 26 hours. Tissues were postfixed in a 1:1 solution of 2% osmium tetrachloride: 3% potassium ferrocyanide at 4°C overnight, rinsed with 0.1 mol/L sodium cacodylate, and dehydrated in graded alcohol solutions before embedding in Embed 812 (Electron Microscopy Sciences, Hatfield, PA). Resin was baked at 60°C for 60 hours. A DiATOME (Hatfield, PA) diamond knife was used to cut 90-nm sections, which were imaged on a JEM 1400 Digital Capture Transmission Electron Microscope (Jeol. Peabody, MD). Morphometrics were assessed in high-quality sections containing full crypts. At least 20 crypts were assessed per mouse by a single blinded observer. The number of granules per cell, percentage of granules that were hypodense, and average number of autophagic vesicles per cell were counted as described.[2,36]

Zinpyr-1 Immunofluorescence

The terminal ileum (n = 4/genotype) was frozen in tissue-freezing medium (Tissue-Tek OCT; Fisher Scientific) floated in an isopropanol/dry ice bath. Sections (10 μm) were cut using a CM 1950 cryostat (Leica), and the fluorescent reporter Zinpyr-1 (ZP1; Toronto Research Chemicals, North York, Ontario) was used to detect labile Zn pools within secretory granules as previously described.[26,37] Images were obtained at 40× magnification using Leica Application Suite (V3.6) on a Leica DM IL LED microscope with a Leica DFC425 digital camera. Brightness was adjusted uniformly across all images using Adobe Photoshop CS3 version 10.0.

Zn Analysis

Zn concentrations of plasma (n = 3/genotype) and small intestine (n = 6/genotype) were determined by atomic absorption spectrophotometry (Aanalyst 400; Perkin Elmer, Waltham, MA) as described.[38]

Crypt Isolation

Intestinal crypts were isolated from mouse small intestine by shaking as described by Ayabe et al.[4] Briefly, 0.5- to 1-cm segments of the entire length of the small intestine were opened longitudinally and exposed to ice-cold EDTA (2 mmol/L) in calcium- and magnesium-free PBS for 30 minutes at 4°C, with gentle agitation. The supernatant was discarded and replaced with cold PBS free of EDTA, which was pipetted vigorously to remove the villous portion. After further resuspension and pipetting, the crypt-enriched portion was filtered through a 70-μm cell strainer (BD Biosciences, San Jose, CA) to remove remaining villi, and centrifuged at 700 × g for 2 minutes to remove single cells. The pelleted crypts were resuspended in Ringer's solution (154 mmol/L NaCl, 2.5 mmol/L KCl, 1 mmol/L $MgSO_4(7H_2O)$, 1 mmol/L $CaCl_2(2H_2O)$, 10 mmol/L HEPES, 10 mmol/L glucose) for exposure to monochloramine (50 μmol/L); in buffered sucrose (0.179 mol/L sucrose, 10 mmol/L Tris–HCl pH 7.4, 1 mmol/L EDTA, 0.75 mmol/L KCl, 19.2 mmol/L NaCl, and protease inhibitors) for sucrose gradient fractionation; or in homogenization buffer (20 mmol/L HEPES pH 7.4, 1 mmol/L EDTA, 250 mmol/L sucrose, and protease inhibitors) for immunoblotting. Crypts for sucrose gradient fractionation or immunoblotting subsequently were dounce homogenized, centrifuged at 1000 × g for 5 minutes, and either used immediately or stored at -20°C.

Subcellular Fractionation

Sucrose gradient fractionation was performed as described previously.[39] Briefly, dounce-homogenized crypts resuspended in buffered sucrose (0.179 mol/L sucrose, 0.75 mmol/L KCl, 19.2 mmol/L NaCl, 1 mmol/L EDTA, and protease inhibitors at pH 7.4) were gently layered on a prepared 0.2–1.6 mol/L sucrose gradient, and centrifuged at 40,000 × g for 18 hours at 4°C. Fractions of 0.5 mL were collected, diluted 2-fold with Tris-buffer (10 mmol/L Tris-HCl and protease inhibitors, pH 7.4), and centrifuged at 150,000 × g for 30 minutes at 4°C to pellet membrane proteins. Membrane proteins were resuspended in homogenization buffer (20 mmol/L HEPES pH 7.4, 1 mmol/L EDTA, 250 mmol/L sucrose, and protease inhibitors) and used for immunoblotting as described later.

Immunoblotting

Tissue homogenates were generated, electrophoresed, and detected by immunoblotting as previously described.[25,31] Primary antibodies used were as follows: 1 μg/mL ZnT2, 1:1000 Reg-IIIγ, or 1:10,000 lysozyme (ab108508; Abcam). Where indicated, membranes were stripped and reprobed using rabbit anti-mouse β-actin (1:5000, 123M4887V; Sigma-Aldrich) as a normalization control. Band density was measured using the Odyssey Image Studio (version 2.0; LI-COR Biosciences, Lincoln, NE). Where appropriate, data represent the mean ratio of band density to β-actin, normalized to background ± SD.

Bactericidal Assay

Enteropathogenic *Escherichia coli* (EPEC) (strain E2348/69 obtained from Dr Lars Bode, University of California San Diego, San Diego, CA) was used for a bactericidal assay as

described by Heneghan et al.[40] Mice (n = 9/genotype) were fasted for 2 hours before euthanization by CO_2 asphyxiation. Terminal ilea (3 cm) were harvested, gently perfused with 1 mL PBS to clear intestinal contents, which were discarded, and an additional 1 mL was perfused through and collected. Bacteria (10 μL containing 3 $\times$ 10^3 colony-forming units [CFU]) was added to 200 μL of intestinal perfusate or PBS and incubated for 1 hour at 37°C. Bacteria were plated in duplicate on Luria-Bertani agar plates and cultured under aerobic conditions for 24 hours at 37°C. CFUs were counted and the number of CFUs cultured from the ileal perfusate from *ZnT2ko* mice was compared with the number of CFUs cultured from the ileal perfusate from *wt* mice. Data represent the mean percentage reduction in CFUs compared with controls (EPEC incubated with PBS only) ± SD.

Monochloramine Exposure and Crypt Viability

Intestinal crypts were harvested as described earlier, resuspended in Ringer's solution, and used immediately. Monochloramine (NH_2Cl) was prepared as described.[41] Crypts were exposed to 50 μmol/L NH2Cl for 1 hour at 37°C, centrifuged at 700 $\times$ g for 2 minutes, and allowed to recover for 1 hour in Ringer's solution at 37°C. To monitor cell death, crypt preparations were exposed to calcein-AM (1.25 μmol/L; excitation, 492 nm; emission, 515 nm; BD Biosciences), and ethidium homodimer-1 (5 μmol/L; excitation, 530 nm; emission, 590 nm; Sigma-Aldrich) for 30 minutes at 37°C in the dark, centrifuged at 700 $\times$ g for 5 minutes, and resuspended in Ringer's solution. The fluorescence was measured in a 96-well fluorimeter (BioTek, Winooski, VT), and cell death was calculated as the ratio of dead (ethidium homodimer-1–stained) to live (calcein-AM–stained) cells for each sample, and then the ratio of cell death in monochloramine-treated cells compared with untreated cells was calculated for each mouse. Data represent the mean cell death of monochloramine-treated cells compared with untreated crypt cells of *wt* and *ZnT2ko* mice ± SD.

Bacteriologic Culture of Mesenteric Lymph Nodes

Mesenteric lymph nodes were isolated and processed for bacteriologic culture as previously described.[42–44] Briefly, lymph nodes from *wt* (n = 6) and *ZnT2ko* (n = 6) mice injected IP with LPS (n = 3) or saline (n = 3) were isolated under sterile conditions and immediately placed into 500 μL Ringer's solution on ice. Lymph nodes then were homogenized, and 100 μL was plated on LB agar plates in duplicate and cultured under aerobic conditions for 24 hours at 37°C. CFUs were counted and summarized as the mean number CFUs per mouse ± SD. Comparisons were reported between the number of CFUs cultured from lymph nodes harvested from *wt* mice and from *ZnT2ko* mice, including those harvested under control conditions and those harvested after mice were treated with LPS.

Splenic Cytokines

TNFα and IL6 concentrations in homogenized spleens taken from mice described earlier were determined by enzyme-linked immunosorbent assay according to the manufacturer's protocol (mouse DuoSet; R&D Systems, Minneapolis, MN). Samples were run in duplicate and data are summarized as the mean cytokine concentration normalized to spleen weights ± SD.

Statistical Analysis

Data are presented as means ± SD. Statistical comparisons were performed using the Student *t* test or 2-way analysis of variance where appropriate (Prism GraphPad, Berkeley, CA), and a significant difference was shown at a *P* value of less than .05.

Fecal Microbiota Analysis by 16s Ribosomal RNA Gene Sequencing

Fresh fecal material was collected and transferred directly into sterile tubes, which were stored at -80°C until further use. Nucleic acid extraction was performed on approximately 0.3 g of mouse feces (n = 14/*ZnT2ko*, 15/*wt*) using a MoBio power fecal DNA isolation kit (MoBio, Carlsbad, CA) following the manufacturer's instructions. The beadbeating step was performed in the Disruptor Genie cell disruptor (Scientific Industries, Bohemia, NY). Genomic DNA was eluted in 50 μL of 10 mmol/L Tris. Illumina (San Diego, CA) iTag PCR reactions (25 μL) contained approximately 20 ng of template DNA and a final concentration of 1$\times$ PCR buffer, 0.8 mmol/L deoxynucleoside triphosphate, 0.625 U Taq polymerase, 0.2 μmol/L 515F forward primer, and 0.2 μmol/L Illumina 806R reverse-barcoded primer per reaction. PCR was performed on a MJ Research PTC-200 thermocycler (Bio-Rad, Hercules, CA) using the following cycling conditions: 98°C for 3 minutes; 35 cycles of 98°C for 1 minute, 55°C for 40 seconds, and 72°C for 1 minute, 72°C for 10 minutes, and kept at 4°C. PCR products were visualized on a 1% CYBRsafe E-gel (Life Technologies, Carlsbad, CA). Pooled PCR products were gel purified using the Qiagen Gel Purification Kit (Qiagen, Frederick, MD), quantified using the Qubit 2.0 Fluorometer (Life Technologies), and samples were pooled in equimolar amounts. Before submission for sequencing, libraries were quality checked using the 2100 Bioanalyzer DNA 1000 chip (Agilent Technologies, Santa Clara, CA). Pooled libraries were stored at -20°C until they were shipped on dry ice to California State University (Northridge, CA) for sequencing. Library pools were size verified using the Fragment Analyzer CE (Advanced Analytical Technologies, Inc, Ames, IA) and quantified using the Qubit high-sensitivity double-stranded DNA kit (Life Technologies). After dilution to a final concentration of 1 nmol/L containing 10% PhiX V3 library control (Illumina), the library pools were denatured for 5 minutes in an equal volume of 0.1 N NaOH, further diluted to 12 pmol/L in HT1 buffer (Illumina), and sequenced using an Illumina MiSeq V2 300 cycle kit cassette with 16S ribosomal RNA library sequencing primers and set for 150 base, paired-end reads. Single-end sequence reads were trimmed at a length of 150 bp and quality filtered at an expected error rate of less than 1.5% using USEARCH v7.[45] After quality filtering, reads were analyzed using the Quantitative Insights into Microbial

Ecology (QIIME) 1.9.0 (Boulder, CO).[46,47] Chimeric sequences were identified using USEARCH61 (Tiburon, CA).[48] A total of 428,301 sequences were retrieved after quality filtering and chimera checking. Open reference operational taxonomic units (OTUs) were picked using the USEARCH7 algorithm,[48] and taxonomy assignment was performed using the Greengenes 16S ribosomal RNA gene database (http://greengenes.secondgenome.com) (13-5 release, 97%).[49] Clustered taxa were compiled into an OTU table, and samples with fewer than 1000 OTUs subsequently were discarded, generating high-quality data from 29 samples (14/*ko*, 15/*wt*).

Microbiota Data Analysis

Principal coordinates analysis plots and Analysis of Familiarity tests for significance were generated from a weighted UniFrac distance matrix made within QIIME 1.9.0. The nonparametric Kruskal–Wallis test for significance was used to identify enriched taxa within *ZnT2ko* and *wt* mice. Differences were considered to be significant at an α value of .025. Relative abundance plots were produced from a cumulative sum scaling normalized OTU table.[50] Linear discriminant analysis effect size was used to identify taxonomic biomarkers between *wt* and *ZnT2ko* mice.[51] Genus-level relative abundances were multiplied by 1 million and formatted as described by Segata et al.[51] Comparisons were made with grouping (*ZnT2ko* or *wt*) as the main categoric variable. α levels of .10 were used for the Kruskal–Wallis tests. Linear discriminant analysis scores for the enriched taxa within each class were plotted. A linear discriminant analysis determines the magnitude of variation between groups. Features were plotted on a logarithmic scale according to the experimental group to which they are significantly associated. Linear discriminant analysis effect size explicitly requires all pairwise comparisons to reject the null hypothesis for detecting the biomarker taxa; thus, no multiple testing corrections were needed.[51]

All authors had access to the study data and reviewed and approved the final manuscript.

Results

ZnT2 Is Present in Secretory Granules of Paneth Cells

We used a set of complementary techniques to detect ZnT2 in PC granules. First, we used IF as shown in Figure 1*A*

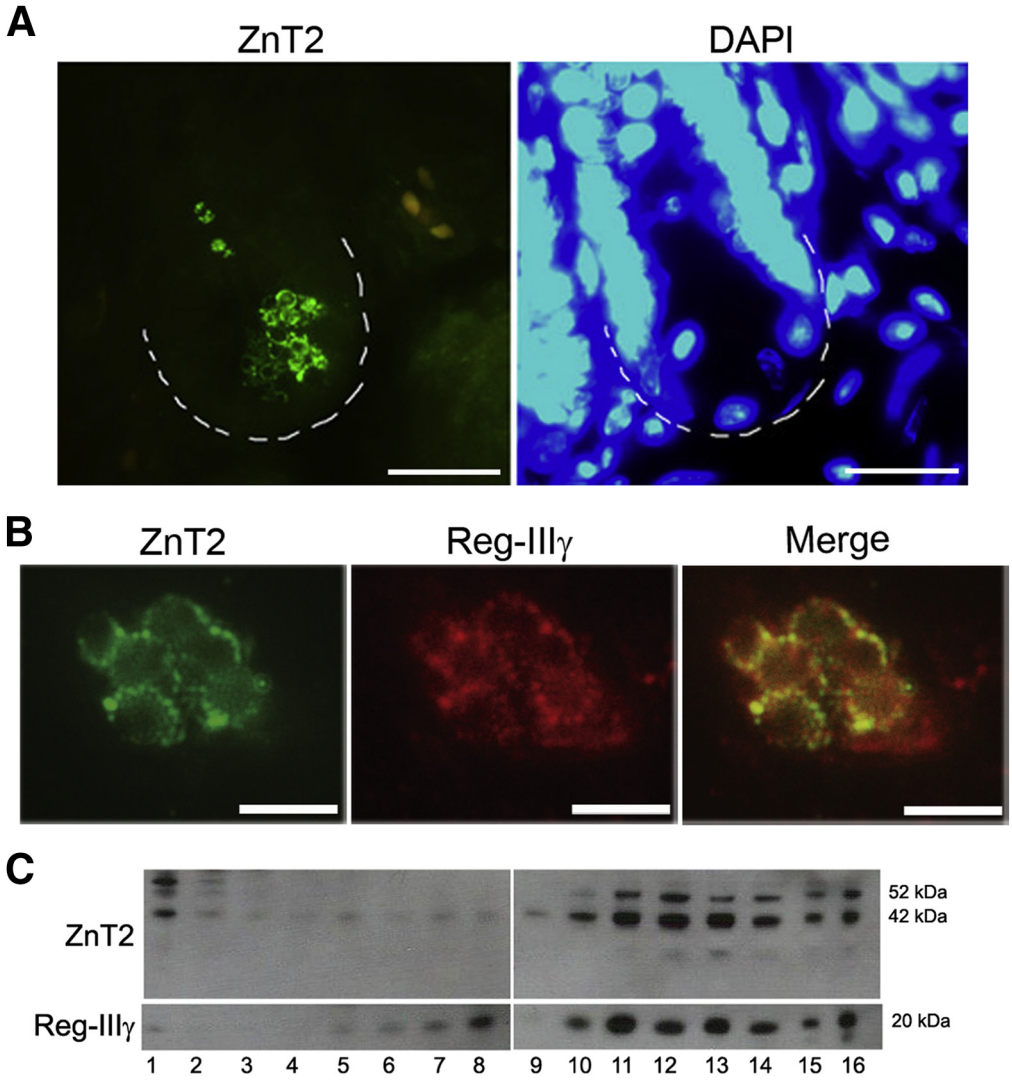

Figure 1. ZnT2 localization in the PCs. (*A*) Representative IF of ZnT2 (green) and nuclei (4',6-diamidino-2-phenylindole [DAPI], blue) in the intestinal crypts of *wt* mice. ZnT2 staining was found only in the crypts of Lieberkühn in a distinct vesicular pattern. Magnification under oil, 63×. *Scale bar*: 20 μm; n = 4/genotype. (*B*) IF of ZnT2 (green) and Reg-IIIγ (red). Overlay image shows vesicular colocalization of ZnT2 and Reg-IIIγ. Magnification under oil, 63×. *Scale bar*: 5 μm; n = 4/genotype. (*C*) ZnT2 and Reg-IIIγ from harvested crypt cells separated by sucrose density gradient centrifugation colocalize within the same subcellular compartments. Fractions 1–16 of increasing density.

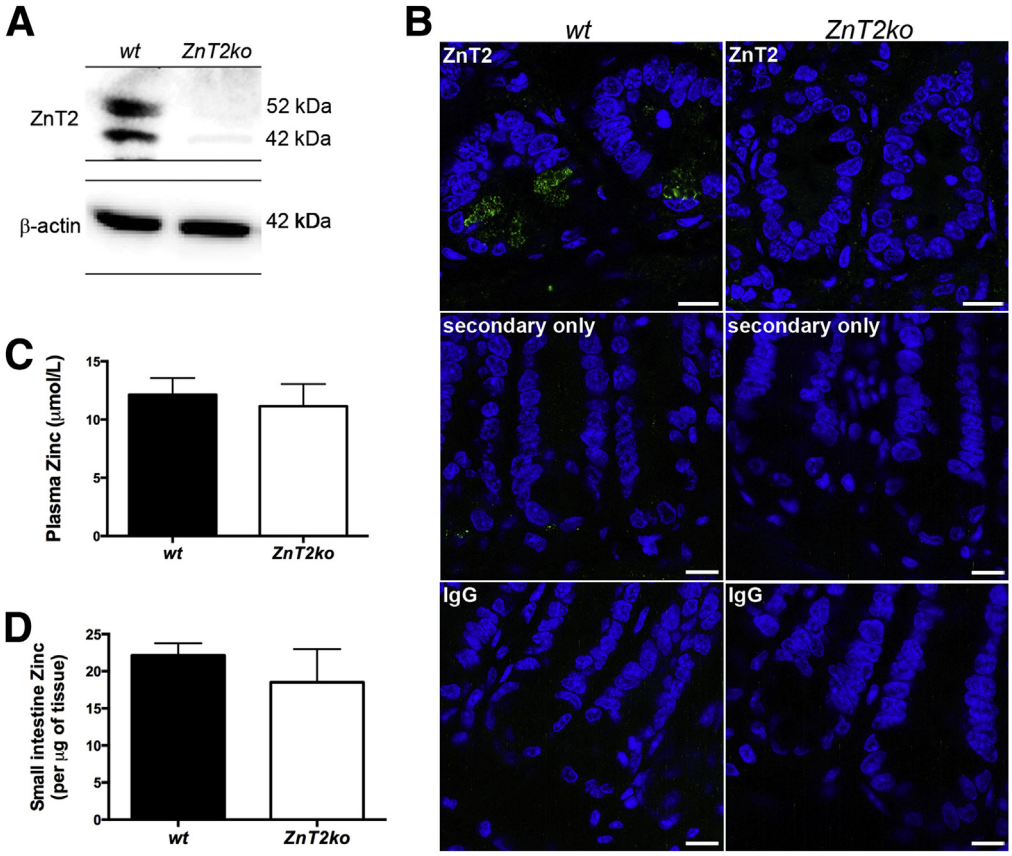

Figure 2. Characterization of *ZnT2ko* mouse Zn profile. (*A*) Representative immunoblot for ZnT2 (and β-actin loading control) in harvested crypts of *wt* and *ZnT2ko* mice. (*B*) IF of ZnT2 (green), nuclei (4',6-diamidino-2-phenylindole [DAPI], blue), and secondary only and nonspecific IgG negative controls in the intestinal crypts of the *wt* and *ZnT2ko* mice. Magnification under oil, 63×. *Scale bar*: 10 μm; n = 4/genotype. (*C*) Plasma Zn. Data represent mean plasma Zn concentration of *wt* and *ZnT2ko* mice ± SD (n = 3/genotype, $P = .5$). (*D*) Small intestine Zn. Data represent small intestine Zn concentrations ± SD (n = 6/genotype, $P = .12$).

and *B*. ZnT2 was detected primarily in the PCs and specifically in membranes of their distinctive secretory vesicles. In addition, we found that ZnT2 was co-localized with Reg-IIIγ (Figure 1*B*), a bactericidal lectin produced and secreted by PCs that binds peptidoglycan carbohydrate moieties expressed by gram-positive bacteria,[5,52] indicating that ZnT2 was localized to PC granules. We confirmed co-localization of ZnT2 and Reg-IIIγ in secretory granules isolated by sucrose density gradient centrifugation (Figure 1*C*).

Overall Histology and Small-Intestine Morphometrics Are Not Altered in ZnT2-Null Mice

Knockout of ZnT2 was confirmed by PCR genotyping (data not shown), immunoblotting of crypt proteins (Figure 2*A*), and IF imaging of the ileum (Figure 2*B*). We noted that ZnT2-null mice were not Zn deficient as assessed by serum Zn levels (Figure 2*C*), and Zn levels in the terminal ileum were not affected significantly (Figure 2*D*). We did not observe differences in gross mucosal structure as assessed by ileal morphometric indices such as crypt depth, villus height/width, cell type, and distribution (Figure 3*A*–*D*) between *wt* and *ZnT2ko* mice. Finally, we did not observe alterations in the number or intracrypt distribution of stem cell populations (Figure 3*E* and *F*), which are thought to be governed by PC function.[53] These observations indicate that deletion of ZnT2 does not lead to systemic disturbances in Zn handling by the organism or disorganization of the cell populations and structure of the mucosa of the small intestine.

Mice Lacking ZnT2 Have Altered Paneth Cell Secretory Granule Morphology and Fail to Accumulate Zn

Standard histology with H&E staining was used to detect and count the eosinophilic PC granules (Figure 4*A*). By using the method of Adolph et al[2] (Figure 4*B*), we found that significantly greater PCs were degranulated in *ZnT2ko* mice when compared with PCs in *wt* mice ($P < .01$) (Figure 4*C*). Qualitatively, we noted that the granules in the PCs of *ZnT2ko* mice appeared disorganized and more variable in size when compared with the PCs of *wt* mice. We confirmed these observations at the ultrastructural level, using transmission electron microscopy. As shown in Figure 5*A*, the PCs in *wt* mice were well organized with tightly packed granules oriented toward the apical membrane that were electron-dense, and relatively uniform in appearance. In contrast, the PCs in *ZnT2ko* mice had fewer loosely packed and hypodense granules (Figure 5*B*–*D*). In addition, there was visual evidence of autophagic vacuolar accumulation and cytoplasmic inclusions, distended endoplasmic reticulum (ER) indicative of ER stress, and fusion of secretory granules indicative of crinophagy[36] (Figure 5*E*). Lastly, we found that PC granules in *ZnT2ko* mice did not accumulate Zn. By using

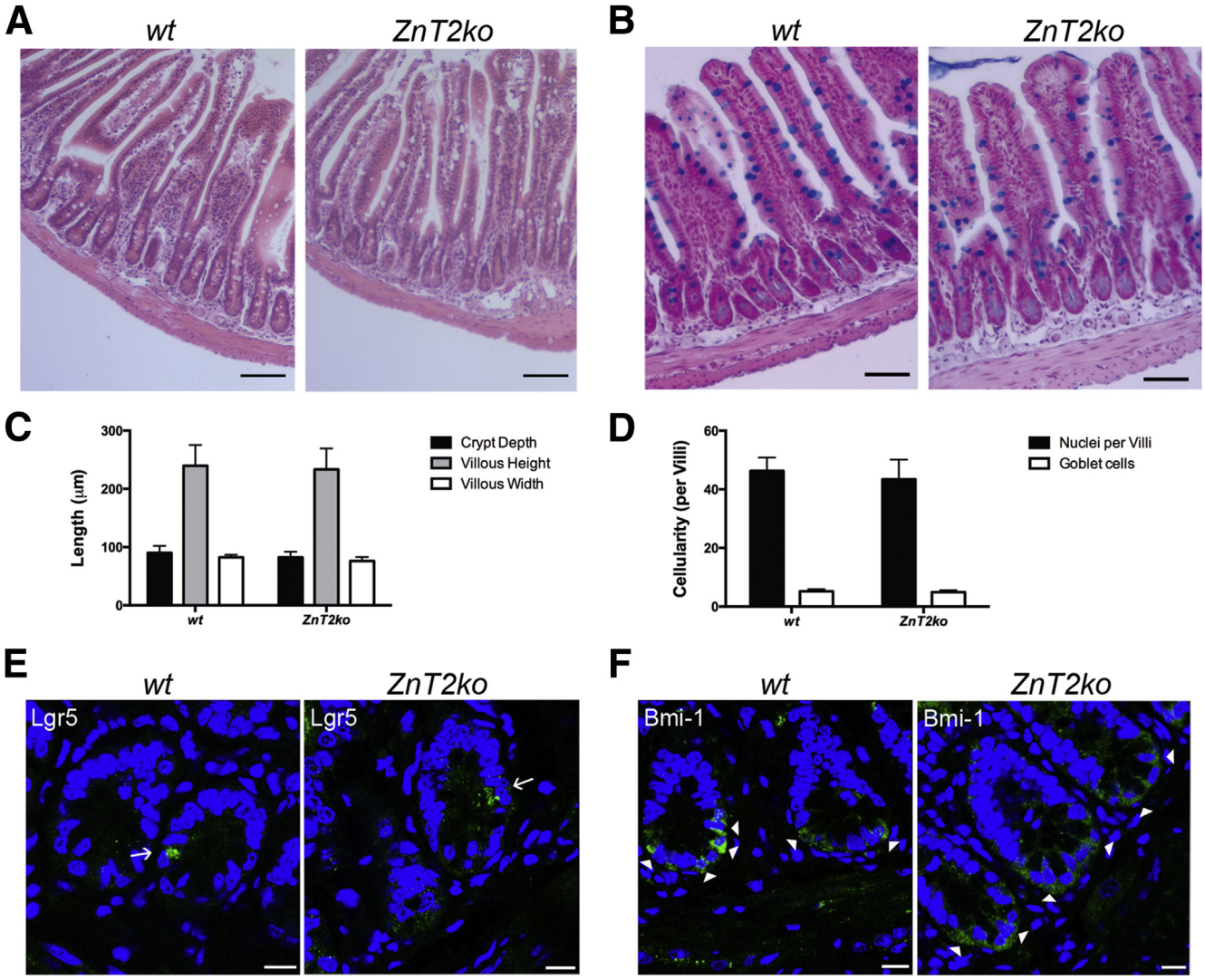

Figure 3. Small intestinal morphology. (*A*) H&E stain and (*B*) alcian blue stain for goblet cells of *wt* and *ZnT2ko* mouse ileum. Magnification, 20×. *Scale bar*: 50 μm. (*C*) Graphic representation of crypt depth, villous height, and crypt width, and (*D*) number of intestinal epithelial cells and goblet cells per villi. No significant differences were observed. Data represent mean measurements and counts (n = 6/genotype; unpaired Student *t* test; mean ± SD). (*E*) Representative IF of Lgr5 (green, denoted by *arrows*) and (*F*) Bmi-1 stem cells (*arrowheads*, green) and nuclei (4',6-diamidino-2-phenylindole [DAPI], blue) in *wt* and *ZnT2ko* crypts. Magnification under oil, 63×. *Scale bar*: 10 μm, n = 2/genotype.

the Zn-responsive fluorophore ZP1, which has a high affinity for labile Zn pools (dissociation constant = 0.7 nmol/L),[54] we detected labile Zn in PC granules of *wt* mice, specifically at the bases of the intestinal crypts (Figure 6). In contrast, ZP1 fluorescence was not observed in the crypt base in the *ZnT2ko* mice, providing direct evidence that Zn does not accumulate in the absence of ZnT2. These observations suggest that loss of Zn transporting capability into the secretory granule of the PC through ZnT2 has 2 consequences: disorganization of secretory granule trafficking and cellular stress.

Fecal Microbiota Is Enriched in Bacteroidales S24-7 in ZnT2-Null Mice

PCs regulate microbial colonization of the intestinal lumen through secretion of their granules.[6] We sought to determine if the compromised secretion of granule products into *ZnT2ko* mice resulted in alterations in the gut microbiota. Weighted UniFrac (distance metric for comparing biologic communities) principal coordinates analysis plots of *wt* and *ZnT2ko* fecal samples showed that overall bacterial community structure was not statistically different between the mouse cohorts (ANOSIM *P* value = .122) (Figure 7*A*). However, relative abundance plots showed differences in community structure at the family level taxonomic ranking (Figure 7*B*). A key observation was that in *wt* mice, several taxa considered integral to the homeostasis of the healthy microbiota including *Ruminococcaceae*, *Ruminococcus*, *Clostridiaceae*, and *Methylobacterium* were enriched.[55] In contrast, members of the *Bacteroidales S24-7* family were found in greater abundance in *ZnT2ko* mice (Figure 7*C*). Collectively, these alterations suggest that the

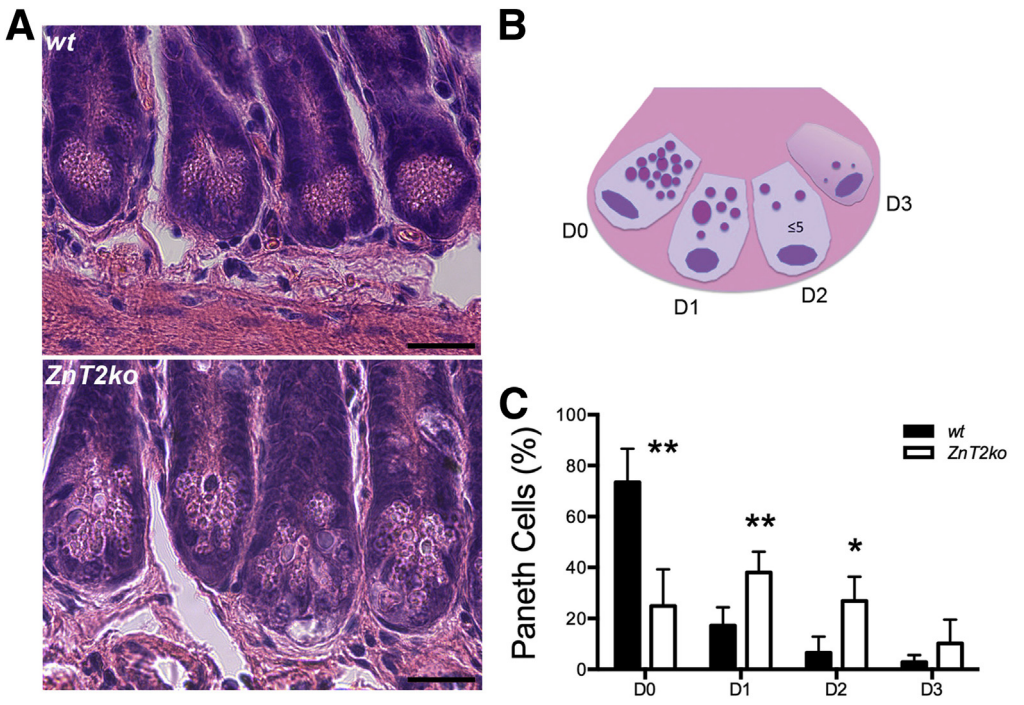

Figure 4. PC histologic measures. (*A*) H&E stain of *wt* and *ZnT2ko* mouse terminal ilea. Magnification: 40×. *Scale bar*: 20 μm; n = 6/genotype. (*B*) Graphic representation of PC degranulation grading scheme (adapted from Adolph et al[2]). (*C*) Percentage baseline degranulation present in PCs of unstimulated ilea. Significantly more *ZnT2ko* PCs were degranulating or depleted (**$P < .01$, *$P < .05$). Data represent the mean number of PCs per crypt quantified according to granule allocation patterns (n = 6 mice/genotype; unpaired Student *t* test; mean ± SD).

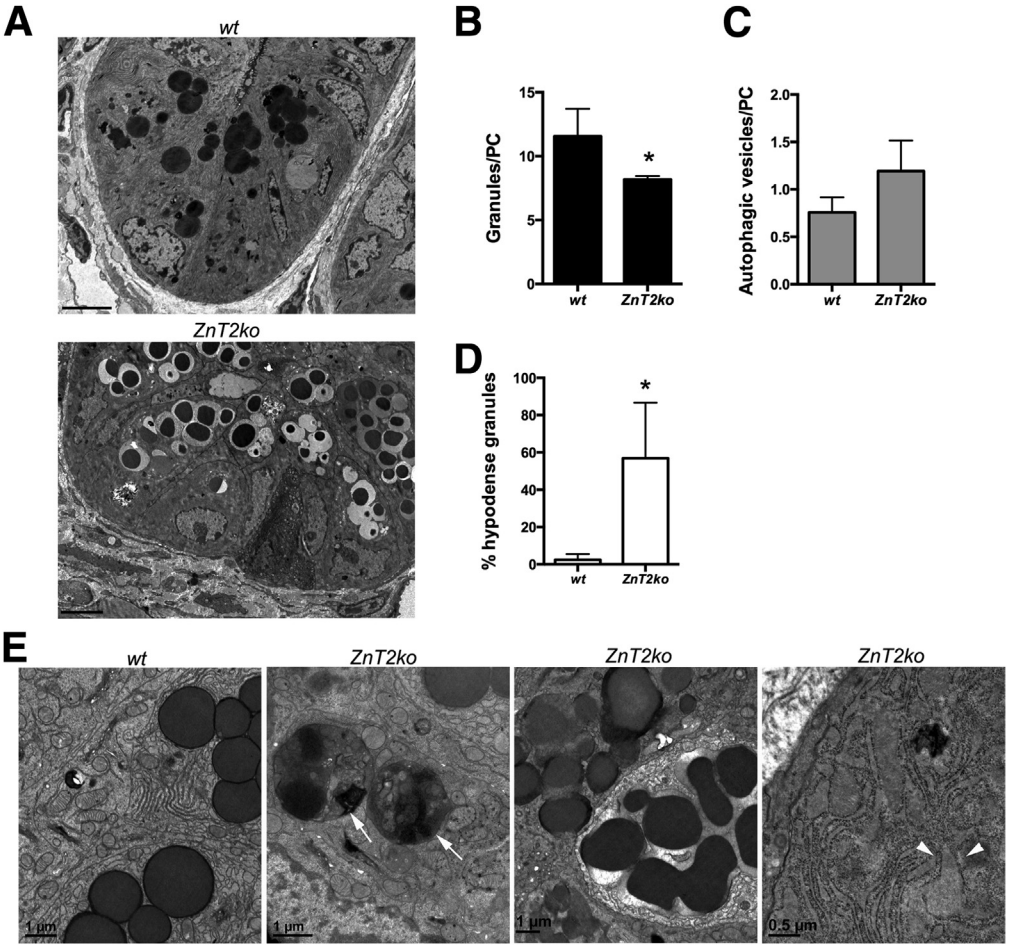

Figure 5. Transmission electron microscopy ultrastructural variation in the crypts of *wt* and *ZnT2ko* mice. (*A*) Representative TEM images showing crypt of *wt* mice with electron-dense, apically oriented granules, and *ZnT2ko*, with abnormal granules. Magnification, 500×. *Scale bar*: 5 μm; n = 4/genotype. (*B*) Mean number of granules per PC (*$P < .05$), (*C*) number of autophagic vesicles per PC ($P = .052$), and (*D*) percentage of hypodense granules present (*$P < .05$). Data represent mean counts (n = 4/genotype; unpaired Student *t* test; mean ± SD). (*E*) Abundant ER and characteristic granules of a *wt* PC, and images showing autophagosomes (*arrows*), a reduced number of abnormal secretory granules undergoing crinophagy, and dilated ER (*arrowheads*) in the PCs of *ZnT2ko* mice. Magnification, 1500–4000×.

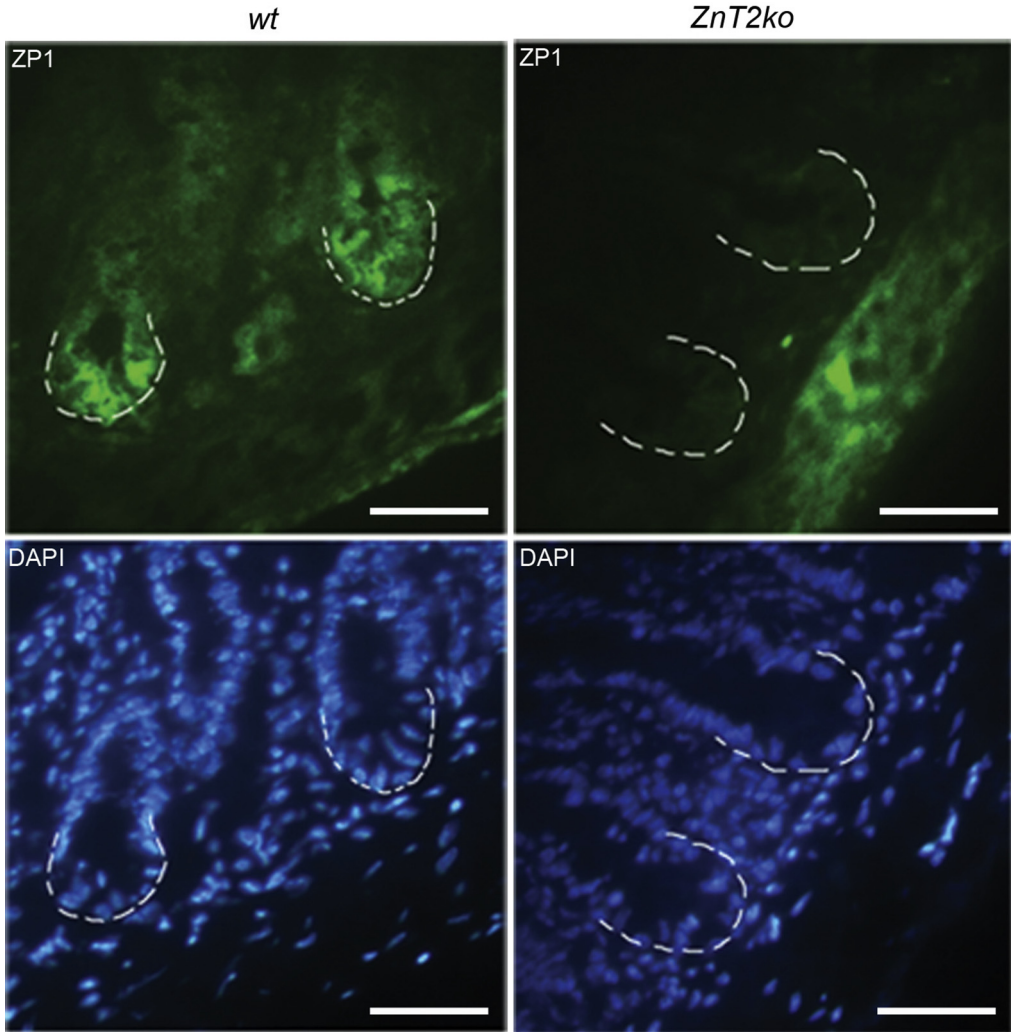

Figure 6. Accumulation of labile Zn in PC secretory granules. ZP1 staining (green, Zn responsive fluorophore) and 4',6-diamidino-2-phenylindole (DAPI) (blue, nuclear counterstain) of *wt* and *ZnT2ko* ilea. Crypt bases are indicated by the *white dotted lines*. Magnification, 40×. *Scale bars*: 20 μm; n = 4/genotype. In the *wt*, ZP1 was observed concentrated in the crypt-base cells. This concentrated localization of staining was absent in the *ZnT2ko* crypts.

loss of ZnT2 alters select species of the colonizing microbiota, which may in turn lead to increased susceptibility to inflammation and infection.

Antipathogen Activity of PC Granules Is Impaired in ZnT2-Null Mice

Lysozyme content of ileum and in luminal fluid itself has been used as a representative protein to monitor the antipathogen capability of the mucosa and its responses to pathogen stress in the lumen.[56,57] In addition, the ratio of lysozyme dimer (less active) to monomer (more active) may provide insight into the antipathogen effectiveness of PC secretions.[10,11] In *ZnT2ko* mice, as compared with *wt* mice, we observed less total lysozyme retained in the mucosa of the terminal ileum ($P < .01$) (Figure 8*A* and *B*), but greater total lysozyme in ileal perfusates ($P < .05$) (Figure 8*C*), suggesting that *ZnT2ko* mice have difficulty regulating secretion of their granules, constitutively releasing increased lysozyme. Of interest, the ratio of lysozyme dimer to monomer also was higher in *ZnT2ko* mice, suggesting that although more lysozyme is released by the mucosa in *ZnT2ko* mice, the PC secretions may be less effective against pathogens (Figure 8*D*) ($P < .05$). To confirm this conjecture, ileal perfusates isolated from *wt* and *ZnT2ko* mice were inoculated with EPEC and incubated for 1 hour at 37°C, then the solutions were plated and cultured for 24 hours and the remaining EPEC colonies were counted. ZnT2-null mice had significantly greater CFUs compared with *wt* mice ($P < .05$), suggesting less antibacterial activity (Figure 9*A*). These findings confirm that PC secretions from *ZnT2ko* mice have compromised bactericidal activity.

Secretion of ZnT2-Null PCs Is Diminished in Response to E coli *Endotoxin*

The secretory response to systemically administered bacterial endotoxin (LPS) has been used to assess PC capabilities to respond to systemic pathogen stress.[4,33] To determine if stimulated secretion was altered in *ZnT2ko* mice, we injected mice with LPS and evaluated PC degranulation at the ultrastructural level (Figure 9*B*). Sections from *wt* mice injected with LPS in vivo showed morphologic characteristics of active degranulation, with apically oriented granules being released into the lumen. This was not observed in the *ZnT2ko* mice; instead PCs appeared

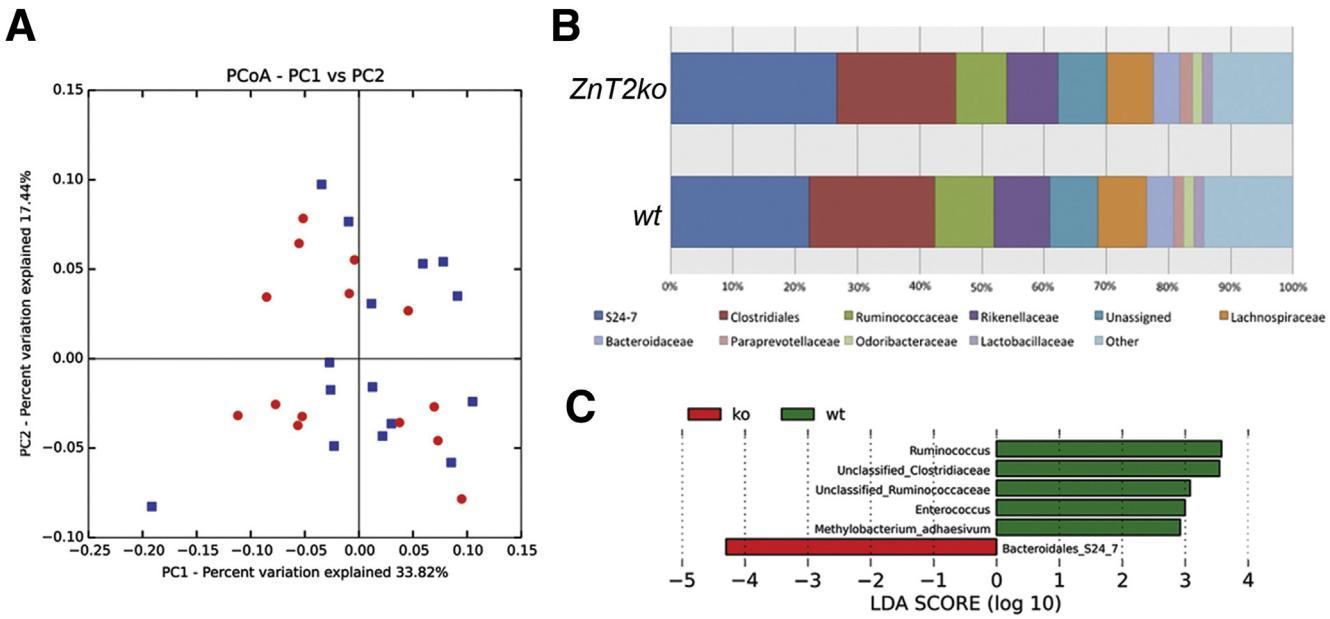

Figure 7. Microbiota of *ZnT2ko* mice. (*A*) Weighted principal coordinates analysis (PCoA) plots generated an unrarifed organizational taxonomic unit table that underwent cumulative sum scaling normalization within QIIME 1.9.0 to visualize differences in bacterial community structure between *wt* (blue, n = 15) and *ZnT2ko* (red, n = 14) mouse fecal samples. Distinct clustering between sample types was not observed; the ANOSIM significance test yielded a *P* value of .122. (*B*) Relative abundance of taxa at the family taxonomic rank based on an unrarified OTU table that underwent CSS normalization within QIIME 1.9.0. The top 10 taxa observed in greatest abundance across all samples (*wt*, n = 15; and *ZnT2ko*, n = 14) are shown. All remaining taxa were grouped into an "other" category. (*C*) Taxa significantly enriched in *ZnT2ko* (red) and *wt* mice (green). Features were plotted on a logarithmic scale according to the experimental group to which they were significantly associated. Linear discriminant analysis (LDA) effect size uses Kruskal–Wallis tests to determine significantly different taxonomic features ($\alpha \leq .10$) between the genotypes.

damaged, with edematous cytoplasm, dilated ER, and altered granule morphology, suggesting that the loss of ZnT2 leads to the inability to activate PC granule secretion and necrotic cell death in response to pathogenic bacteria.

Loss of ZnT2 Reduces Crypt Viability in Response to Monochloramine Exposure

Monochloramine (NH_2Cl) is a molecule generated in the presence of neutrophil-derived hypochlorous acid and bacteria-derived ammonia.[58] Thus, we next sought to determine whether the loss of ZnT2 would cause oxidative stress or increase susceptibility to oxidants generated by microbial stress. We found that loss of ZnT2 did not affect baseline levels of oxidative stress, as indicated by quantification of 8-hydroxydeoxyguanosine–positive nuclei (*wt*, 33 ± 14 nuclei/field; *ZnT2ko*, 43 ± 20 nuclei/field); however, there was significantly greater cell death ($P < .05$) in response to NH_2Cl in crypts isolated from *ZnT2ko* mice compared with *wt* mice (Figure 9*C*). This suggests that mice lacking ZnT2 are more susceptible to oxidative stress generated in the setting of local inflammation.

Loss of ZnT2 Increases Bacterial Translocation and Splenic Cytokine Production in Response to LPS

To determine if mice lacking ZnT2 might have an altered response to infection, we injected mice with LPS and evaluated mesenteric nodes for bacterial translocation after 24 hours[4] (Figure 10*A*). A 2-factor analysis of variance showed a significant effect of genotype. *ZnT2ko* mice had greater bacterial translocation across the ileal wall, with a higher number of bacterial colonies cultured from mesenteric lymph nodes ($P < .05$). Moreover, LPS injection significantly increased bacterial translocation ($P < .05$) in *ZnT2ko* mice, whereas the effect in *wt* mice did not reach significance.

In addition, to determine if *ZnT2ko* mice had an altered local inflammatory response to LPS treatment, proinflammatory splenic cytokines, TNF-α and IL6, were quantified by enzyme-linked immunosorbent assay (Figure 10*B* and *C*). A 2-factor analysis of variance showed a significant effect of genotype. There was evidence of a more intense systemic innate immune response in *ZnT2ko* mice, as evidenced by greater concentration of both TNFα ($P < .05$) and IL6 ($P = .07$) in the spleens of *ZnT2ko* mice in response to LPS. These findings suggest that mice lacking ZnT2 show increased mucosal permeability and heightened local inflammatory response to bacterial products (LPS).

Discussion

PCs have a distinct requirement for Zn, and defects in Zn metabolism have been implicated previously in PC dysfunction.[8,12,37] The demand for Zn by the PC appears to be satisfied through the activity of the apical membrane Zn

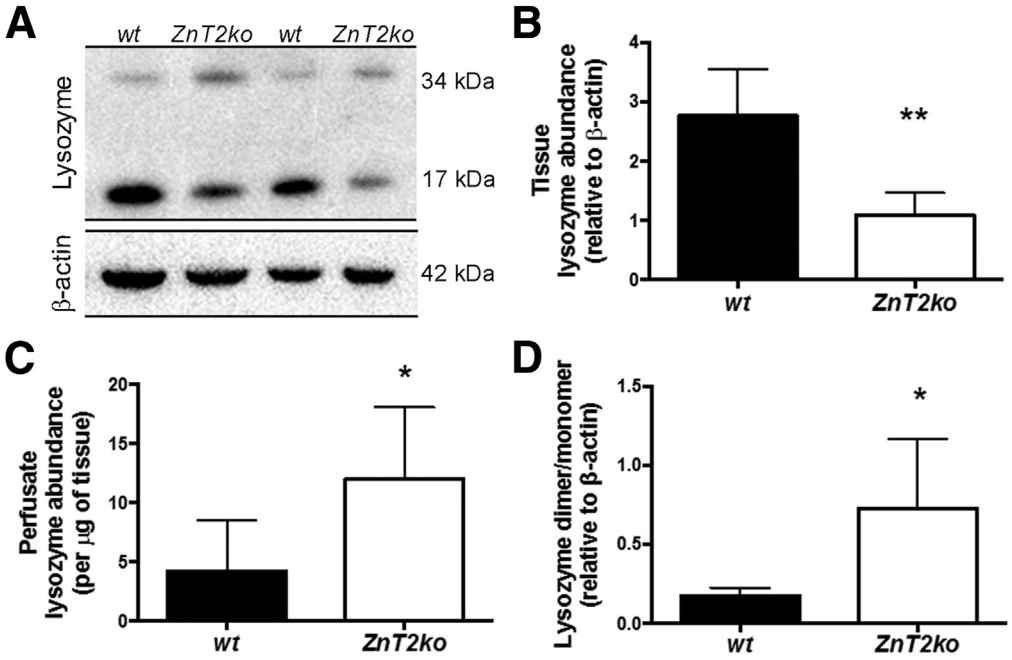

Figure 8. Lysozyme secretion in *ZnT2ko* mice. (*A*) Representative immunoblot for lysozyme (and β-actin loading control) in harvested ileal segments from *wt* and *ZnT2ko* mice after perfusion with saline. (*B*) Lysozyme abundance in the ilea of *wt* and *ZnT2ko* mice. *ZnT2ko* mice had significantly less lysozyme overall (n = 6/genotype, $^{**}P < .01$). (*C*) Lysozyme release into the small intestinal lumen at baseline. In unstimulated ileum, the *ZnT2ko* released relatively greater lysozyme in comparison with the *wt* (n = 6/genotype, $^{*}P < .05$). (*D*) Ratios of dimeric to monomeric lysozyme were increased significantly in the ilea of *ZnT2ko* mice (n = 6/genotype, $^{*}P < .05$). Immunoblots were performed in duplicate.

transporter Zrt-Irt-like protein 4 (ZIP4).[13] Acrodermatitis enteropathica, a genetic disorder of severe Zn deficiency, is caused by mutations in the gene that encodes ZIP4 (*SLC39A4*), resulting in loss of ZIP4 function, is characterized by chronic diarrhea and susceptibility to infections, providing evidence of the clinical importance of this Zn requirement in the PC.[59] Although the importance of the ZIP4-mediated pathway for Zn transport into the PC is apparent, the pathways of intracellular Zn distribution and transport into the PC granules have not been characterized, and their influence on health is not known.

Previous reports noted that ZnT2 messenger RNA is expressed robustly in the small intestine[29] and a small ZnT2 isoform (~28 kilodaltons) is associated with the apical membrane in enterocytes[27] of the duodenum and jejunum. In the ileum, minimal ZnT2 expression is detected, and only in the cells of the crypts.[27] In the present study, we have shown that expression of the larger vesicular ZnT2 isoforms (~42 and 52 kilodaltons)[60] is restricted to PCs, and is responsible for Zn accumulation into PC granules. Although the smaller ZnT2 isoform may play a role in Zn export in times of Zn excess, the vesicular isoforms have been shown to play a role in coordinated secretory processes, such as those described in the mammary gland[25] and characteristic of PCs.

In this context, this study provides 3 principal sets of observations on the functional significance of ZnT2 in the PC. The first is that disruption of ZnT2-mediated Zn accumulation into granules profoundly affected PC morphology, including granule disorganization, swollen ER indicative of ER stress, and degradation of the granules themselves (crinophagy), a feature of Crohn's disease,[36] stages of starvation,[61] and Zn deficiency.[62] Loss of ZnT2 did not lead to signs of global Zn deficiencies or toxicities in the mice or disturbances in the neighboring stem cell niche. PCs, although they are thought to regulate many important stem cell functions,[53] may be disrupted without damaging the stem cell niche.[63] The second is that functional silencing of ZnT2 altered the steady-state intestinal microbiome and impaired the response of PCs to bacterially generated endotoxin and pathogenic bacteria themselves. The third is that loss of ZnT2 increased the susceptibility of the PC to toxic products of gut inflammation such as monochloramine. An additional preliminary observation is that loss of ZnT2 seems to impair the functional barrier to bacterial translocation and enhanced innate immune responses during the response to a systemic septic challenge. Together these observations provide confidence in the conclusion that the ZnT2 pathway of Zn transport influences homeostasis in the environment of the intestinal lumen through its regulation of PC secretions and resilience to pathogenic conditions.

With respect to the mechanisms by which ZnT2-mediated accumulation of Zn in the secretory granule leads to a loss of cellular integrity, there are 2 general explanations. The first is that, as a member of the ZnT family that exports Zn from the cytoplasm, ZnT2 may be important for buffering against the toxic effects of Zn accumulation in the cytoplasm.[64] Arguing against this explanation would be that accumulation of free cytoplasmic Zn was not observed in PCs; however, it remains unknown if toxic accumulation

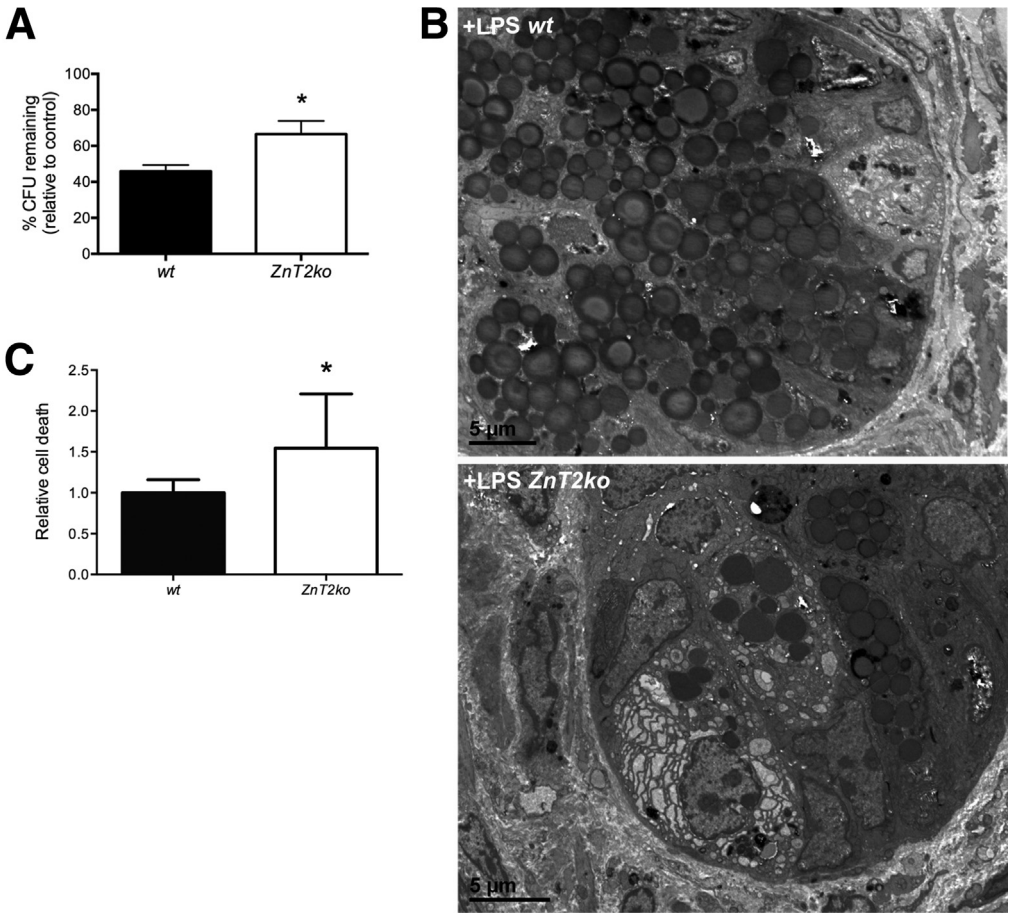

Figure 9. Susceptibility to microbial products. (*A*) *ZnT2ko* mice showed a lower percentage reduction in CFUs compared with controls (EPEC incubated with PBS only) compared with *wt* (n = 9/genotype, $^*P < .05$; unpaired Student *t* test; mean ± SD). (*B*) After injection of LPS, representative transmission electron microscopy images of *wt* PCs with increased numbers of apical granules being released into the lumen, whereas *ZnT2ko* PCs appeared damaged, with edematous cytoplasm, dilated ER, and altered granule morphology (magnification, 600×; n = 3/genotype). (*C*) Significant increase in cell death in the *ZnT2ko* in response to NH_2Cl (n = 8/genotype, $^*P < .05$; unpaired Student *t* test; mean ± SD).

of Zn occurred in other organelles that might serve as sinks for Zn accumulating abnormally in the cytoplasm. An alternative explanation is that ZnT2 might play a role in granule stability, as has been recognized in other cell types including kidney fibroblasts[65] and the lactating mammary gland.[26] Toxicities of Zn accumulation or the instability of granules might lead to downstream consequences favoring events such as free radical formation and oxidative stress, as has been observed in mammary glands[26]; or activation of pathways of autodegradation and apoptosis leading to abnormal turnover, as has been observed in gastric parietal cells.[58] Along these lines, it is noteworthy that cell death was enhanced when crypts were exposed to monochloramine, an oxidant generated during inflammation from bacteria-derived ammonia and neutrophil-derived reactive oxygen species.[41,58] These considerations indicate that impairment of ZnT2 activity impairs resilience of the PC to oxidant stress generated from outside sources and from cellular metabolism. Studies pursuing such hypotheses are not within the scope of the current study, but would be useful to more fully understand how derangements in cellular management of Zn lead to impairment of signature functions and cell viability in specialized, slow-turnover secretory cells such as PCs.

The presence of ZnT2-mediated Zn transport in the PC granule may play several roles in regulating antipathogen functions: PCs respond to microbial products and inflammatory cytokines, maintaining the normal microbiota[66,67] and protecting against luminal pathogens.[33,57] Zn recently was shown to stabilize α-defensins (cryptdins in mice)[9] and maintain lysozyme in its more active monomeric state.[11] Consistent with this, we found that the loss of granule Zn led to less monomeric lysozyme retained within the PC, and granule contents were not released in a coordinated manner. It seems likely that other constituents of the PC granule are influenced by the absence of Zn, including the cryptdins[9]; matrix metalloproteinase 7, which requires Zn as a cofactor; and TNFα, which is present within PC granules[3] and is processed by a Zn-requiring TNF-α–converting enzyme to produce its secreted form.[68,69] Importantly, impaired ability to package and secrete PC granules in *ZnT2ko* mice rendered PCs less able to regulate the balance between pathogenic and nonpathogenic bacterial populations in the lumen. Increased abundance of members of the Bacteroidales family, including the S24-7 isolate identified in our study, has been observed in other conditions of PC dysfunction[6] and has been identified as a possible indicator of disease onset in colitis models.[70] In human beings, loss of this PC-regulated balance among microbe populations has been implicated in compromised barrier function, mucosal inflammation syndromes such as NEC and Crohn's disease, long-term risks for malignancy, and even obesity.[6]

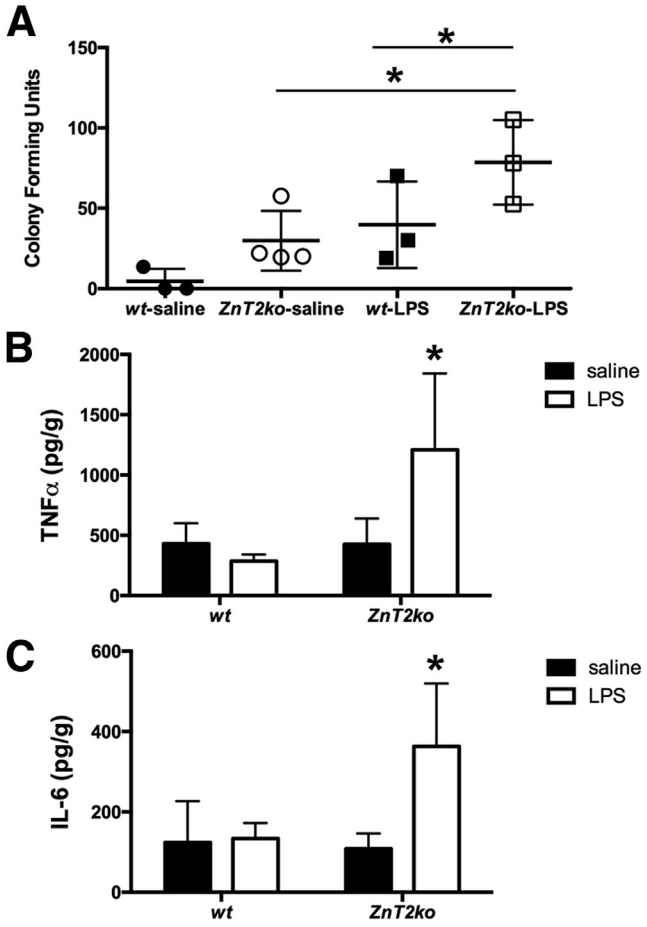

Figure 10. Inflammatory response to LPS. (*A*) Significant increase in bacterial translocation to mesenteric lymph nodes in *ZnT2ko* mice in response to LPS (n = 3/treatment group, **P* < .05; 2-way analysis of variance; mean ± SD). (*B* and *C*) ZnT2-null mice responded with significant production of TNFα and IL6 compared with *wt* mice in response to LPS (n = 3/treatment group, **P* < .05; 2-way analysis of variance; mean ± SD).

With such potentially broad health consequences connected to proper functioning of ZnT2, it would be of great interest to know whether genetic variants in its gene (*SLC30A2*) are common in the general population. In this regard, functional mutations and nonsynonymous genetic variants with diverse functional consequences have been identified in different human populations, most notably in lactating women.[30–32] These considerations offer the possibility that subtle, but functionally significant, genetic variations in ZnT2 may contribute to the diversity of responses in human populations in diseases associated with gut dysbiosis.

In summary, the current study identifies the transporter ZnT2 as a driver of Zn uptake and storage in the PC granule, with consequences for PC granule structure and secretion, and, importantly, for regulation of the balance between pathogenic and nonpathogenic bacteria in the intestine. We propose that loss of ZnT2 function and subsequent PC dysfunction could lead to broad deficits in overall gut function and susceptibility to infectious and inflammatory conditions. It remains to be determined if the loss of ZnT2 function in human beings is associated with microbial dysbiosis and subsequent inflammatory bowel diseases.

References

1. Clevers HC, Bevins CL. Paneth cells: maestros of the small intestinal crypts. Annu Rev Physiol 2013;75:289–311.
2. Adolph TE, Tomczak MF, Niederreiter L, et al. Paneth cells as a site of origin for intestinal inflammation. Nature 2013;503:272–276.
3. Schmauder-Chock EA, Chock SP, Patchen ML. Ultrastructural localization of tumour necrosis factor-alpha. Histochem J 1994;26:142–151.
4. Ayabe T, Satchell DP, Wilson CL, et al. Secretion of microbicidal alpha-defensins by intestinal Paneth cells in response to bacteria. Nat Immunol 2000;1:113–118.
5. Brandl K, Plitas G, Schnabl B, et al. MyD88-mediated signals induce the bactericidal lectin RegIII gamma and protect mice against intestinal Listeria monocytogenes infection. J Exp Med 2007;204:1891–1900.
6. Salzman NH, Bevins CL. Dysbiosis–a consequence of Paneth cell dysfunction. Semin Immunol 2013;25:334–341.
7. Lewin K. The Paneth cell in health and disease. Ann R Coll Surg Engl 1969;44:23–37.
8. Elmes ME, Jones JG. Paneth cell zinc: a comparison of histochemical and microanalytical techniques. Histochem J 1981;13:335–337.
9. Zhang Y, Cougnon FB, Wanniarachchi YA, et al. Reduction of human defensin 5 affords a high-affinity zinc-chelating peptide. ACS Chem Biol 2013;8:1907–1911.
10. During K, Porsch P, Mahn A, et al. The non-enzymatic microbicidal activity of lysozymes. FEBS Lett 1999;449:93–100.
11. Chakraborti S, Chatterjee T, Joshi P, et al. Structure and activity of lysozyme on binding to ZnO nanoparticles. Langmuir 2010;26:3506–3513.
12. Sawada M, Takahashi K, Sawada S, et al. Selective killing of Paneth cells by intravenous administration of dithizone in rats. Int J Exp Pathol 1991;72:407–421.
13. Geiser J, Venken KJ, De Lisle RC, et al. A mouse model of acrodermatitis enteropathica: loss of intestine zinc transporter ZIP4 (Slc39a4) disrupts the stem cell niche and intestine integrity. PLoS Genet 2012;8:e1002766.
14. Zhang C, Sherman MP, Prince LS, et al. Paneth cell ablation in the presence of Klebsiella pneumoniae induces necrotizing enterocolitis (NEC)-like injury in the small intestine of immature mice. Dis Model Mech 2012;5:522–532.
15. Lichten LA, Cousins RJ. Mammalian zinc transporters: nutritional and physiologic regulation. Annu Rev Nutr 2009;29:153–176.
16. Kambe T, Hashimoto A, Fujimoto S. Current understanding of ZIP and ZnT zinc transporters in human health and diseases. Cell Mol Life Sci 2014;71:3281–3295.
17. Golan Y, Berman B, Assaraf YG. Heterodimerization, altered subcellular localization, and function of multiple zinc transporters in viable cells using bimolecular

fluorescence complementation. J Biol Chem 2015; 290:9050–9063.
18. Kambe T. An overview of a wide range of functions of ZnT and Zip zinc transporters in the secretory pathway. Biosci Biotechnol Biochem 2011;75:1036–1043.
19. Kelleher SL, McCormick NH, Velasquez V, et al. Zinc in specialized secretory tissues: roles in the pancreas, prostate, and mammary gland. Adv Nutr 2011;2:101–111.
20. Palmiter RD, Cole TB, Quaife CJ, et al. ZnT-3, a putative transporter of zinc into synaptic vesicles. Proc Natl Acad Sci U S A 1996;93:14934–14939.
21. Lemaire K, Ravier MA, Schraenen A, et al. Insulin crystallization depends on zinc transporter ZnT8 expression, but is not required for normal glucose homeostasis in mice. Proc Natl Acad Sci U S A 2009;106:14872–14877.
22. Chimienti F, Devergnas S, Pattou F, et al. In vivo expression and functional characterization of the zinc transporter ZnT8 in glucose-induced insulin secretion. J Cell Sci 2006;119:4199–4206.
23. Yu YY, Kirschke CP, Huang L. Immunohistochemical analysis of ZnT1, 4, 5, 6, and 7 in the mouse gastrointestinal tract. J Histochem Cytochem 2007;55:223–234.
24. Murgia C, Vespignani I, Cerase J, et al. Cloning, expression, and vesicular localization of zinc transporter Dri 27/ZnT4 in intestinal tissue and cells. Am J Physiol 1999;277:G1231–G1239.
25. Lopez V, Kelleher SL. Zinc transporter-2 (ZnT2) variants are localized to distinct subcellular compartments and functionally transport zinc. Biochem J 2009;422:43–52.
26. Lee S, Hennigar SR, Alam S, et al. Essential role for zinc transporter 2 (ZnT2)-mediated zinc transport in mammary gland development and function during lactation. J Biol Chem 2015;290:13064–13078.
27. Liuzzi JP, Bobo JA, Cui L, et al. Zinc transporters 1, 2 and 4 are differentially expressed and localized in rats during pregnancy and lactation. J Nutr 2003;133:342–351.
28. Kelleher SL, Velasquez V, Croxford TP, et al. Mapping the zinc-transporting system in mammary cells: molecular analysis reveals a phenotype-dependent zinc-transporting network during lactation. J Cell Physiol 2012;227:1761–1770.
29. Liuzzi JP, Blanchard RK, Cousins RJ. Differential regulation of zinc transporter 1, 2, and 4 mRNA expression by dietary zinc in rats. J Nutr 2001;131:46–52.
30. Itsumura N, Inamo Y, Okazaki F, et al. Compound heterozygous mutations in SLC30A2/ZnT2 results in low milk zinc concentrations: a novel mechanism for zinc deficiency in a breast-fed infant. PLoS One 2013;8:e64045.
31. Chowanadisai W, Lonnerdal B, Kelleher SL. Identification of a mutation in SLC30A2 (ZnT-2) in women with low milk zinc concentration that results in transient neonatal zinc deficiency. J Biol Chem 2006;281:39699–39707.
32. Alam Samina HSR, Gallagher Carla, Soybel David I, et al. Exome sequencing of SLC30A2 identifies novel loss- and gain-of-function variants associated with breast cell dysfunction. J Mammary Gland Biol Neoplasia 2015; 20:159–172.
33. Rumio C, Sommariva M, Sfondrini L, et al. Induction of Paneth cell degranulation by orally administered Toll-like receptor ligands. J Cell Physiol 2012;227:1107–1113.
34. Helmrath MA, Fong JJ, Dekaney CM, et al. Rapid expansion of intestinal secretory lineages following a massive small bowel resection in mice. Am J Physiol Gastrointest Liver Physiol 2007;292:G215–G222.
35. Wittkopf N, Gunther C, Martini E, et al. Lack of intestinal epithelial atg7 affects paneth cell granule formation but does not compromise immune homeostasis in the gut. Clin Dev Immunol 2012;2012:278059.
36. Thachil E, Hugot JP, Arbeille B, et al. Abnormal activation of autophagy-induced crinophagy in Paneth cells from patients with Crohn's disease. Gastroenterology 2012; 142:1097–1099 e4.
37. Giblin LJ, Chang CJ, Bentley AF, et al. Zinc-secreting Paneth cells studied by ZP fluorescence. J Histochem Cytochem 2006;54:311–316.
38. Clegg MS, Keen CL, Lonnerdal B, et al. Influence of ashing techniques on the analysis of trace elements in biological samples: II. Dry ashing. Biol Trace Elem Res 1981;3:237–244.
39. Kelleher SL, Lonnerdal B. Mammary gland copper transport is stimulated by prolactin through alterations in Ctr1 and Atp7A localization. Am J Physiol Regul Integr Comp Physiol 2006;291:R1181–R1191.
40. Heneghan AF, Pierre JF, Tandee K, et al. Parenteral nutrition decreases paneth cell function and intestinal bactericidal activity while increasing susceptibility to bacterial enteroinvasion. JPEN J Parenter Enteral Nutr 2014;38:817–824.
41. Prasad M, Matthews JB, He XD, et al. Monochloramine directly modulates Ca(2+)-activated K(+) channels in rabbit colonic muscularis mucosae. Gastroenterology 1999;117:906–917.
42. Garcia-Tsao G, Lee FY, Barden GE, et al. Bacterial translocation to mesenteric lymph nodes is increased in cirrhotic rats with ascites. Gastroenterology 1995;108: 1835–1841.
43. Berg RD, Garlington AW. Translocation of certain indigenous bacteria from the gastrointestinal tract to the mesenteric lymph nodes and other organs in a gnotobiotic mouse model. Infect Immun 1979;23:403–411.
44. Diehl GE, Longman RS, Zhang JX, et al. Microbiota restricts trafficking of bacteria to mesenteric lymph nodes by CX(3)CR1(hi) cells. Nature 2013;494: 116–120.
45. Edgar RC. UPARSE: highly accurate OTU sequences from microbial amplicon reads. Nat Methods 2013; 10:996–998.
46. Caporaso JG, Kuczynski J, Stombaugh J, et al. QIIME allows analysis of high-throughput community sequencing data. Nat Methods 2010;7:335–336.
47. Caporaso JG, Lauber CL, Walters WA, et al. Global patterns of 16S rRNA diversity at a depth of millions of sequences per sample. Proc Natl Acad Sci U S A 2011; 108(Suppl 1):4516–4522.
48. Edgar RC. Search and clustering orders of magnitude faster than BLAST. Bioinformatics 2010;26:2460–2461.
49. DeSantis TZ, Hugenholtz P, Larsen N, et al. Greengenes, a chimera-checked 16S rRNA gene database and workbench compatible with ARB. Appl Environ Microbiol 2006;72:5069–5072.

50. Paulson JN, Stine OC, Bravo HC, et al. Differential abundance analysis for microbial marker-gene surveys. Nat Methods 2013;10:1200–1202.
51. Segata N, Izard J, Waldron L, et al. Metagenomic biomarker discovery and explanation. Genome Biol 2011;12:R60.
52. Vaishnava S, Yamamoto M, Severson KM, et al. The antibacterial lectin RegIIIgamma promotes the spatial segregation of microbiota and host in the intestine. Science 2011;334:255–258.
53. Sato T, van Es JH, Snippert HJ, et al. Paneth cells constitute the niche for Lgr5 stem cells in intestinal crypts. Nature 2011;469:415–418.
54. Chang CJ, Nolan EM, Jaworski J, et al. Bright fluorescent chemosensor platforms for imaging endogenous pools of neuronal zinc. Chem Biol 2004;11:203–210.
55. Antharam VC, Li EC, Ishmael A, et al. Intestinal dysbiosis and depletion of butyrogenic bacteria in Clostridium difficile infection and nosocomial diarrhea. J Clin Microbiol 2013;51:2884–2892.
56. Peeters T, Vantrappen G. The Paneth cell: a source of intestinal lysozyme. Gut 1975;16:553–558.
57. Farin HF, Karthaus WR, Kujala P, et al. Paneth cell extrusion and release of antimicrobial products is directly controlled by immune cell-derived IFN-gamma. J Exp Med 2014;211:1393–1405.
58. Kohler JE, Dubach JM, Naik HB, et al. Monochloramine-induced toxicity and dysregulation of intracellular Zn2+ in parietal cells of rabbit gastric glands. Am J Physiol Gastrointest Liver Physiol 2010;299:G170–G178.
59. Lombeck I, von Bassewitz DB, Becker K, et al. Ultrastructural findings in acrodermatitis enteropathica. Pediatr Res 1974;8:82–88.
60. Kelleher SL, Lonnerdal B. Zn transporter levels and localization change throughout lactation in rat mammary gland and are regulated by Zn in mammary cells. J Nutr 2003;133:3378–3385.
61. Hodin CM, Lenaerts K, Grootjans J, et al. Starvation compromises Paneth cells. Am J Pathol 2011;179:2885–2893.
62. Suzuki H, Igarashi Y, Konno T, et al. Inclusion bodies in Paneth cells in zinc deficiency. Lancet 1979;1:734.
63. Shroyer NF, Helmrath MA, Wang VY, et al. Intestine-specific ablation of mouse atonal homolog 1 (Math1) reveals a role in cellular homeostasis. Gastroenterology 2007;132:2478–2488.
64. Palmiter RD, Cole TB, Findley SD. ZnT-2, a mammalian protein that confers resistance to zinc by facilitating vesicular sequestration. EMBO J 1996;15:1784–1791.
65. Kobayashi T, Beuchat MH, Lindsay M, et al. Late endosomal membranes rich in lysobisphosphatidic acid regulate cholesterol transport. Nat Cell Biol 1999;1:113–118.
66. Nieuwenhuis EE, Matsumoto T, Lindenbergh D, et al. Cd1d-dependent regulation of bacterial colonization in the intestine of mice. J Clin Invest 2009;119:1241–1250.
67. Chang SY, Lee SN, Yang JY, et al. Autophagy controls an intrinsic host defense to bacteria by promoting epithelial cell survival: a murine model. PLoS One 2013;8:e81095.
68. Moss ML, Jin SL, Milla ME, et al. Cloning of a disintegrin metalloproteinase that processes precursor tumour-necrosis factor-alpha. Nature 1997;385:733–736.
69. Cross JB, Duca JS, Kaminski JJ, et al. The active site of a zinc-dependent metalloproteinase influences the computed pK(a) of ligands coordinated to the catalytic zinc ion. J Am Chem Soc 2002;124:11004–11007.
70. Schwab C, Berry D, Rauch I, et al. Longitudinal study of murine microbiota activity and interactions with the host during acute inflammation and recovery. ISME J 2014;8:1101–1114.

Received July 26, 2015. Accepted December 22, 2015.

Correspondence
Address correspondence to: Shannon L. Kelleher, PhD, Penn State Hershey College of Medicine, 500 University Drive, Hershey, Pennsylvania 17033. e-mail: slk39@psu.edu; fax: (717) 531-5393.

Acknowledgments
The authors would like to acknowledge Dr Abby K. Geletzke and Sooyeon Lee for technical assistance in preparation of this manuscript. The authors would like to thank the Microscopy and Cytometry Facility of the Huck Institute of the Life Sciences at Penn State, and the Histology, Confocal Microscopy, and Electron Microscopy Core Facilities at Penn State College of Medicine.

Conflicts of interest
The authors disclose no conflicts.

Funding
Supported by intramural support from the Academic Enrichment Fund (S.L.K.) and David L. Nahrwold Endowment (D.I.S.) of the Penn State Hershey Department of Surgery, and work at Juniata College was supported by a grant from the Howard Hughes Medical Institute through the Precollege and Undergraduate Science Education Program and a National Science Foundation award (DBI-1248096).